Hydrological Sciences Journal

ISSN: (Print) (Online) Journal homepage: www.tandfonline.com/journals/thsj20

Improving pluvial flood mapping resolution of large coarse models with deep learning

Cesar Ambrogi Ferreira Do Lago, Jose Artur Teixeira Brasil, Marcus Nóbrega Gomes Junior, Eduardo Mario Mendiondo & Marcio H. Giacomoni

To cite this article: Cesar Ambrogi Ferreira Do Lago, Jose Artur Teixeira Brasil, Marcus Nóbrega Gomes Junior, Eduardo Mario Mendiondo & Marcio H. Giacomoni (2024) Improving pluvial flood mapping resolution of large coarse models with deep learning, Hydrological Sciences Journal, 69:5, 607-621, DOI: 10.1080/02626667.2024.2329268

To link to this article: https://doi.org/10.1080/02626667.2024.2329268

HYDROLOGICAL SCIENCES JOURNAL
2024, VOL. 69, NO. 5, 607–621
https://doi.org/10.1080/02626667.2024.2329268

FEATURED ARTICLE

Improving pluvial flood mapping resolution of large coarse models with deep learning

Cesar Ambrogi Ferreira Do Lago[a], Jose Artur Teixeira Brasil[a], Marcus Nóbrega Gomes Junior[a,b], Eduardo Mario Mendiondo[b] and Marcio H. Giacomoni[a]

[a]Klesse College of Engineering, University of Texas at San Antonio, San Antonio, Texas, USA; [b]WADI Lab - Hydraulics & Sanitary Engineering, University of Sao Paulo, Sao Carlos, Brazil

ABSTRACT

Deep learning (DL) models are a promising complement to hydrodynamic models. However, the application of DL for detailed predictions in large domains has not yet been tested. We aim to narrow this gap by improving flood mapping resolution derived from large coarse flood models. We used cGAN-Flood, a conditional generative adversarial-based model (cGAN), that showed satisfactory generalization. We demonstrate the applicability of cGAN-Flood by coupling it with mesh- and raster-based coarse models. A Hydrologic Engineering Center (HEC) River Analysis System (RAS) model (cell size of 32 m), which is mesh-based, was created for a 350 km^2 watershed. In contrast, a HydroPol2D model, raster-based, was created for a 150 km^2 watershed with a 15 m pixel size. We evaluated our method's performance against a 3 m resolution HEC-RAS model in seven catchments across the cities of San Antonio and Sao Paulo. Results indicate the cGAN-Flood improved flood map accuracy, illustrating how DL can enhance flood mapping resolution.

ARTICLE HISTORY
Received 18 July 2023
Accepted 24 January 2024

EDITOR
A Castellarin

ASSOCIATE EDITOR
A. Domeneghetti

KEYWORDS
deep learning; rapid flood modelling; high-resolution flood mapping; rain-on-grid; artificial neural networks

1 Introduction

Floods are the most expensive natural disasters in terms of human and economic losses (Natarajan and Radhakrishnan 2019, Bulti and Abebe 2020). In particular, concerns regarding pluvial flooding in urban areas have increased in the past two decades (Rangari *et al.* 2018). Although coastal floods and river floods are generally larger and the most durable types of flooding, pluvial flooding may cause more damage to property due to its higher occurrence frequency (Szewrański *et al.* 2018).

Flood modelling is a vital tool for floodplain managers to quantify flood risks and develop mitigation strategies (Do Lago *et al.* 2021). Two-dimensional (2D) hydrodynamic models are the most effective tool for predicting urban pluvial flooding (Bulti and Abebe 2020, Cea and Costabile 2022). However, these models are computationally expensive, limiting their application in large watersheds (hundreds of square kilometres). Traditionally, 2D hydrodynamic models of large areas leverage coarse cell resolution. This approach limits the number of computational nodes, enabling simulations to conclude within a manageable time frame. However, coarser cell resolution reduces the accuracy of flood mapping (Chen *et al.* 2012), especially in urban areas where the local topology is misrepresented (Fewtrell *et al.* 2008).

Rapid flood models (RFMs) can be an alternative to hydrodynamic models. RFMs reduce simulation time by employing simplified hydraulic concepts or rules, such as cellular automata (Wolfram 1984, Jamali *et al.* 2019), instead of solving complex physical equations (Teng *et al.* 2017). HydroPol2D (Gomes *et al.* 2023) is one example of a cellular automata model, which uses Manning's non-linear equation, instead of shallow-water equations (SWEs), for distributing runoff between cells. However, the simplifications assumed for RFM reduce their accuracy when compared to traditional hydrodynamic models. Furthermore, high-resolution simulations may require small time steps, especially when high velocities are simulated within the domain (Guidolin *et al.* 2016), in order to maintain a valid Courant number for numerical stability (Gomes *et al.* 2023). This disadvantage can hamper the application of cellular automata in large domains when the goal is high-resolution mapping.

Deep learning (DL) can be used to model complex hydrodynamic processes while maintaining computational efficiency, and has been applied in flood studies (Berkhahn *et al.* 2019, Dtissibe *et al.* 2020, Kabir *et al.* 2020, Hofmann and Schüttrumpf 2021, Löwe *et al.* 2021). However, while DL-based models have demonstrated promising results in flood prediction, they are usually domain-specific and their capacity to reproduce flood predictions outside the training dataset and under different rainfall conditions is limited. The lack of generalization is still a major challenge for the use of DL models in practical applications (Do Lago *et al.* 2023, Karim *et al.* 2023). The difficulty in generalizing flood predictions can particularly affect the application of DL in large domains, which would require training a single DL model for the entire area or developing numerous distinct models for different locations within the domain. In the case of creating one large model, especially when aiming for high-resolution prediction, the DL model would have to handle a large number of parameters

CONTACT Cesar Ambrogi Ferreira Do Lago cesar-lago@hotmail.com Klesse College of Engineering, University of Texas at San Antonio, One UTSA Circle, San Antonio, Texas, 78249, USA
Supplemental data for this article can be accessed online at https://doi.org/10.1080/02626667.2024.2329268

during the training process. Training such a model would be challenging, as the training process is time consuming and requires a significant amount of data (Bentivoglio *et al.* 2022).

The literature reports recent improvements in DL models' ability to generalize outside the training areas. Löwe *et al.* (2021), for example, trained a U-Net-based DL model on portions of their study area and showed it was capable of predicting floods in unobserved parts of the same catchment. However, the capacity of their model to generalize to other catchments still needs to be evaluated. Guo *et al.* (2022) trained a similar DL model using outputs from Weighted Cellular Automata 2D (WCAD2D) (Guidolin *et al.* 2016), a cellular automata model. Their model satisfactorily predicted maximum water depths and flow velocities in various catchments, but cannot generalize for different rainfall events. Bentivoglio *et al.* (2023) developed a graph neural network inspired by SWE (SWE-GNN), which learned how to distribute water between cells. Their model was tested for a dike breach simulation, showing great generalization capabilities when exposed to new topologies, different breach locations, larger domains, and extended simulation time frames. While SWE-GNN shows great generalization potential, it has only been evaluated under constant breach inflow conditions on randomly generated digital elevation models (DEMs). Its applicability in complex real-world scenarios and different boundary conditions, such as rain-on-grid, remains to be tested. Do Lago *et al.* (2023) used a conditional generative adversarial network (cGAN) for pluvial flood modelling (cGAN-Flood), which was, on average, 250 times faster than the Hydrologic Engineering Center's River Analysis System (HEC-RAS) (Brunner 2016). cGAN-Flood distributes a pre-defined flood volume to generate the flood map and could be generalized to different rainfalls and catchments. However, this model was tested for catchments in San Antonio (Texas) that are smaller than 500 ha. The cGAN-Flood's efficacy in catchments with spatial characteristics distinct from those in San Antonio and its performance of larger domain modelling still needs evaluation.

Despite the advances in the generalization capacity of DL flood models, the applicability of DL models for large domain predictions has not been shown in the literature. To tackle this gap, our study introduces a pioneering application of DL models to enhance the resolution of flood mapping derived from coarse hydrodynamic models created for large domains. We exemplify our methods with two types of coarse flood models, mesh- and raster-based models, which provide cGAN-Flood with the total volume to be redistributed. This approach reveals the potential to enhance the resolution of pluvial flood mapping of pre-existing 2D hydrodynamic models of large watersheds.

2 Methodology

2.1 cGAN-Flood

We applied a DL model to enhance flood mapping resolution from two modelling approaches: raster and mesh-based models. Raster-based models compute the flood dynamics directly between the pixels of the input rasters. Examples of raster-based models are Gridded Surface Subsurface Hydrologic Analysis (GSSHA) (Downer and Ogden 2004), WCA2D (Guidolin *et al.* 2016) and HydroPol2D (Gomes *et al.* 2023). On the other hand, mesh-based models, such as HEC-RAS (Brunner 2016) and Two-dimensional Unsteady FLOW (TUFLOW) (WBM 2016), sub-divide the domain into smaller cells that can account for one or more pixels. Cells in mesh-based models can have different shapes and sizes, while the cells in raster-based models are square, with sizes corresponding to the pixel resolution of the input data. In this paper, we used cGAN-Flood (Do Lago *et al.* 2023) as a DL model to increase the resolutions of flood maps generated from raster- and mesh-based models. This DL model works by distributing a given flood volume over a given area, which can be calculated using low-resolution flood models. It is worth noting that cGAN-Flood can also be combined with a hydrological model for generating flood maps. Do Lago *et al.* (2023) demonstrated how cGAN-Flood could be coupled with the Storm Water Management Model (SWMM) (Rossman 2010). The overall methodology is presented in Fig. 1. cGAN-Flood is based on a conditional generative adversarial network (cGAN). GANs consist of two ANN components: a generator (G) and a discriminator (D), which engage in a competitive training process. The discriminator D is trained to distinguish the output of the generator G from actual data, while G is trained to produce outputs that closely resemble true data (Wang *et al.* 2017, Gonog and Zhou 2019). This approach significantly enhances the generator's ability to create realistic outputs and has been applied in various fields, including vision computing, language processing, and medical applications Wang *et al.* (2017). Traditional GANs utilize random noise as inputs for generating final images, while conditional GANs (cGANs) employ labels to guide generators in producing final outputs. cGAN-Flood uses two generators to distribute a target volume (v_t) across a given catchment to create a map of maximum pluvial flooding depths. The inputs of the model are a DEM, flow accumulation, slope, and imperviousness maps (Fig. 1). A first generator (Generator 1) was trained to learn what cells are likely to be flooded first by creating a rank map with values ranging from −1 to 1, in which cells with larger numbers are characterized by a higher likelihood of being flooded. A threshold τ is applied to this map to identify flooded cells. In this case, a cell is considered wet if its rank exceeds the threshold. Finally, the second generator (Generator 2) calculates the depths of the wet cells to create a depth map. cGAN-Flood enforces a water balance with a search algorithm to identify the optimum threshold value that would produce a depth map with a total flood volume that matches v_t (input volume that the user aims to distribute). Further details on the cGAN-Flood model are given by Do Lago *et al.* (2023).

FoTor generate high-resolution flood maps in large domains, cGAN-Flood was coupled with coarse flood models. This model calculates and routes excess precipitation, providing cGAN-Flood with v_t. In this case, the primary goal is not the hydraulic behaviour (e.g. depth and velocity) of the runoff within these coarser cells, but rather their maximum runoff volume. Although hydrodynamic models may produce

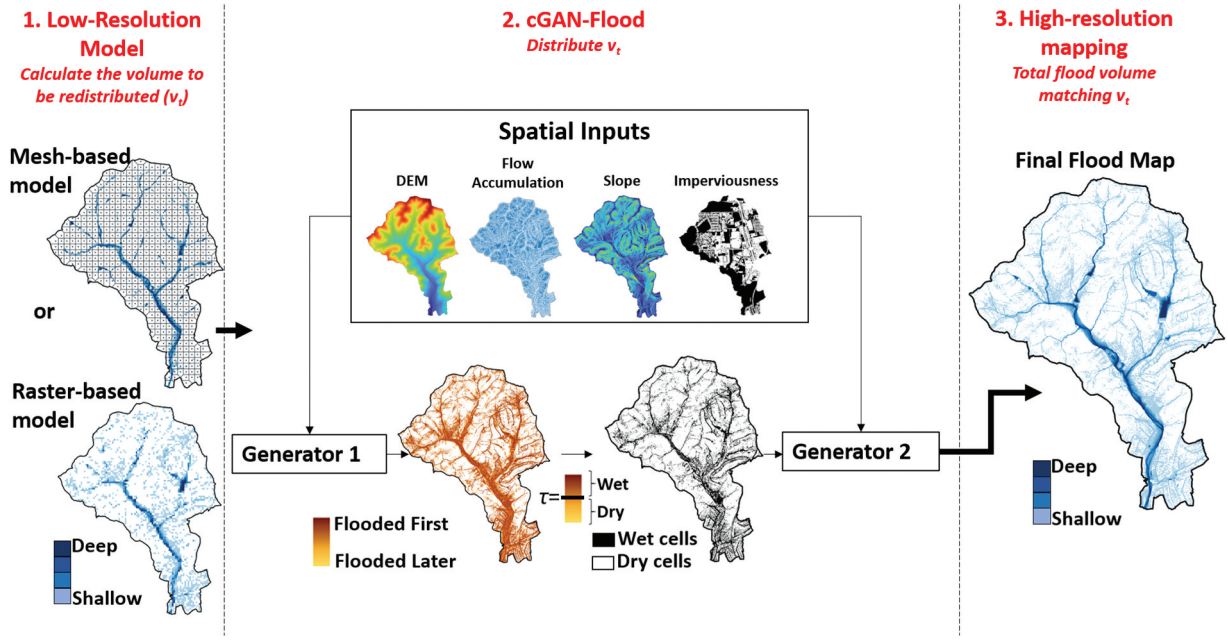

Figure 1. The overall methodology includes the calculation of flood volumes with low-resolution models (1), which are distributed with cGAN-Flood (2) to generate high-resolution flood maps (3).

unrealistic flood maps at low resolutions, they still maintain a proper water balance and flow between cells as a physically-based model, provided that stability issues are addressed. Flow charts demonstrating how we built and coupled low-resolution mesh- and raster-based models with cGAN-Flood are shown in the Supplementary material, parts 1 and 2.

Our study focused on utilizing maximum flood volumes to create maximum flood maps. However, there is potential for temporal analysis to generate flood maps at specific time intervals by using instantaneous flood volumes instead. It is crucial to acknowledge that the frequency of generating these maps directly impacts computational performance. For instance, producing flood maps every minute would have a simulation time 10 times longer compared to generating them every 10 min. Furthermore, it is important to note that the current implementation of the cGAN-Flood model was trained under conditions of increasing flood levels. Consequently, its effectiveness during the receding phase of floods remains unexplored.

2.2 Studied areas

Our methods were applied to two distinct watersheds: the Upper San Antonio (UPSA) watershed in San Antonio, Texas, and the Aricanduva watershed in Sao Paulo, Brazil. For the UPSA, we developed a mesh-based model and coupled it with cGAN-Flood. In contrast, the Aricanduva watershed was modelled with a raster-based model. Therefore, we demonstrate with these two study areas how raster and mesh types of flood model can be combined with cGAN-Flood. Furthermore, the Aricanduva watershed presents spatial characteristics markedly different from those in San Antonio, where cGAN-Flood was trained and tested. The contrasting geographies and characteristics of these two locations are particularly relevant, as they allow us to evaluate the ability of cGAN-Flood to generalize and adapt to diverse spatial inputs.

2.3 Upper San Antonio watershed

First, we applied cGAN-Flood to improve flood mapping resolution from a coarse 2D HEC-RAS model, version 6.2 (Brunner 2016), created for the UPSA watershed. This coarse HEC-RAS model provides cGAN-Flood with the flood volume to be redistributed (v_t) for a high-resolution flood map output. This watershed contains one training, two validation, and two test catchments used for cGAN-Flood development and evaluation (Do Lago *et al.* 2023), shown in Fig. 2(a). Do Lago *et al.* (2023) showed that although most of the training areas are located inside the Leon Creek watershed, cGAN-Flood performed satisfactorily on testing catchments (500 ha) located inside UPSA.

The HEC-RAS domain has an area of approximately 350 km^2 with a base cell size of 100 m. The terrain used for the simulations has a 3 m resolution, resampled from a 1 m resolution DEM provided by the San Antonio River Authority (SARA) (E. Cavazos, personal communication, 2018). Breaklines were added for the reaches with a flow accumulation area larger than 100 ha. We selected a cell size of 15 m for these breaklines to improve the flood dynamics prediction in areas with high flows. We added near repeats so that the 15 m cells cover the entire reach width where necessary. Additional breaklines were added for transportation infrastructure in UPSA watershed. A polyline file with the transportation infrastructure of San Antonio was acquired from the City of San Antonio (2023). Misaligned cell faces can lead to unintended water flow between cells, especially when these faces do not align with high-elevation pixels that signify natural barriers. By adding and enforcing

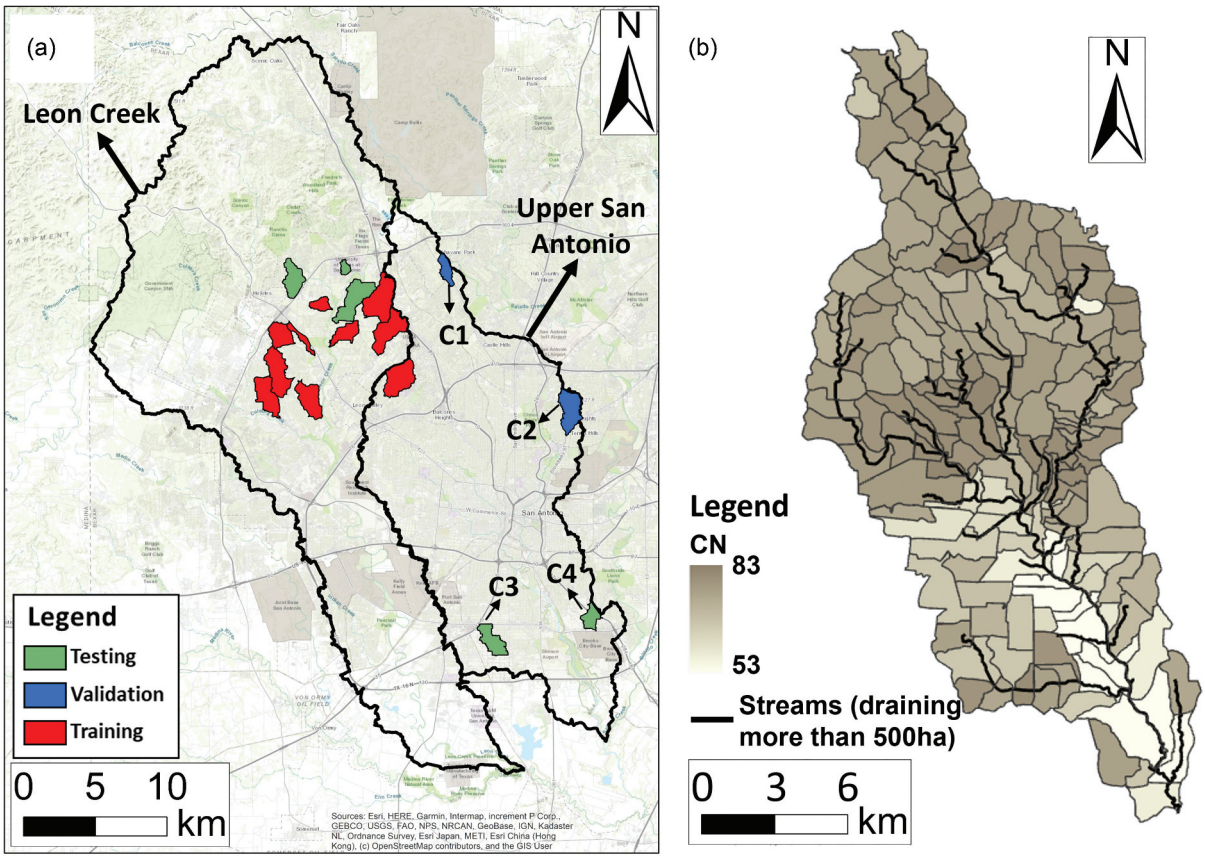

Figure 2. (a) UPSA watershed with cGAN-Flood training, validation and testing areas; and (b) streams, sub-catchments and CN values.

breaklines corresponding to streets and roads, the water flow is better represented with a more accurate v_t used with cGAN-Flood. After adding the breaklines, the average cell size of the HEC-RAS models is 32 m. Furthermore, underground drainage infrastructure, such as culverts and pipes, was burned into the terrain by artificially lowering the surface elevation, with their corresponding width, to allow hydraulic connectivity across the domain. A polyline with the underground drainage system and its characteristics was also downloaded from the City of San Antonio (2023).

We have used Manning's n of 0.035 $m^{1/3}s^{-1}$ for impervious areas and channels and 0.1 $m^{1/3}s^{-1}$ for pervious areas. A 1 m resolution map with imperviousness areas, provided by the San Antonio River Authority (SARA) (E. Cavazos, personal communication, 2018), was also resampled to 3 m. The curve number (CN) was the infiltration method used in this model. The CN values for 155 sub-catchments were acquired from a UPSA HEC-Hydrologic Modeling System (HMS), available at the Digital Data Model Repository (D2MR) website, shown in Fig. 2(b). In this study, no calibration attempts were performed, as the focus of the paper is demonstrating how DL models can be used to improve flood mapping resolution. Despite not calibrating the hydraulic models, the Manning's n within recommended values and CN values that were acquired from SARA's HEC-HMS model makes the HEC-RAS plausible in representing infiltration and overflow conditions. Different model parameterization could affect the v_t values and the final flood maps. However, the methods applied in this paper can be reproduced with any other mesh-based model configuration and parameters.

When applying cGAN-Flood for flood volume redistribution in the UPSA, the process is conducted independently across the 155 HEC-HMS sub-catchments. The total flood volume (v_t) is calculated by summing the volumes of all cells within each sub-catchment. Since mesh cell delineation does not always coincide with sub-catchment borders, cells on the boundaries of two sub-catchments may extend into both areas. To address this, we redraw the sub-catchments to align with cell faces, ensuring each cell lies entirely within a single sub-catchment for the purpose of v_t redistribution. v_t is calculated via elevation–volume tables after acquiring the maximum Water surface elevation (WSE) of each cell. This process is done automatically by reading the hfd plan file of HEC-RAS (see Supplementary material, part 1, for further details).

Notably, cGAN-Flood is focused on predicting pluvial flooding and was neither trained nor tested for areas larger than 500 ha. Due to the different nature and characteristics of fluvial flooding, the cGAN-Flood model is not recommended for such predictions. We conducted previous investigations showing that cGAN-Flood failed to predict flooding in areas with high flow accumulation. Similarly, Löwe *et al.* (2021) developed a DL model to predict pluvial flooding in urban areas, and excluded fluvial flood from their predictions. As such, we did not redistribute fluvial flooding from segments receiving runoff from larger areas. To do so, we exclude fully flooded cells adjacent to a flow line with a flow accumulation exceeding 500 ha (Fig. 2(b))

from the redistribution process. The flood depths for these cells, as determined by the low-resolution HEC-RAS, are maintained in the final maps. Considering that fluvial flooding can be accurately and rapidly simulated with one-dimensional (1D) models, our primary objective is to enhance the resolution of pluvial flood maps, which necessitates 2D modelling.

2.3.1 Analysis of performance in San Antonio catchments

High-resolution HEC-RAS mapping of the whole UPSA was unfeasible due to computational resources and simulation time. Simulating the UPSA with a 3 m cell size would result in approximately 75 million cells, which would not be supported due to a lack of computational memory. In addition, the simulation time would be unpredictable. Therefore, we tested the performance of cGAN-Flood to improve the flood mapping resolution of HEC-RAS model in catchments C1, C2, C3, and C4 (Fig. 2(a)). C1 and C2 were validation areas utilized by Do Lago *et al.* (2023), to identify the optimal parameters for generators 1 and 2 within the cGAN-Flood model. As catchments C1 and C2 were exclusively used for performance metric calculations and not directly seen during the training process, they were also used for assessing our methodology to couple HEC-RAS with cGAN-Flood. HEC-RAS models with a 3 m resolution were created for each catchment to be used as ground truth. Then, coarse HEC-RAS models were created for calculating v_t. The same methodology used for selecting cell sizes, applying breaklines, and adding terrain modifications in UPSA was used in these catchments. The 25-year and 100-year storms, with a 3-h duration (Do Lago *et al.* 2023), were used to evaluate the performances. The rainfall temporal distribution was determined using the alternating blocks method, with a resolution of 5 min. The rainfall used in this paper is spatially uniform.

We simulated the 100-year storm in the whole UPSA to estimate the simulation time of cGAN-Flood and perform a visual comparison between low-resolution HEC-RAS and cGAN-Flood maps. Although we could not compare the whole UPSA with the high-resolution HEC-RAS, simulation time is still a relevant performance metric when simulating large domains.

2.4 Aricanduva watershed

The Aricanduva watershed is located in the city of Sao Paulo, Brazil, and covers an area of approximately 240 km^2 (Fig. 3). The watershed was modelled using HydroPol2D, a raster-based model. HydroPol2D is a diffusive-like cellular automata model that couples hydrological, hydrodynamic, and water quality transport and fate (see Gomes *et al.* 2023 for a detailed model description). It also contains terrain analysis algorithms to treat DEM issues and permit proper hydrological continuity, allowing terrain smoothing (Schwanghart and Scherler 2017) and burning (De Paiva *et al.* 2013).

We used a 15 m resolution for the HydroPol2D simulations. The DEM was resampled from a 1 m resolution map (PMSP 2017), with bridges and culverts manually burned using HEC-RAS terrain modification. The channel modifications were calculated by measuring the channel's width close to the bridge or culvert. The map of permeable and impermeable areas was resampled from a 10 m map (PMSP 2017). The terrain and impervious map resampling operations were performed using the bilinear and nearest neighbour methods.

The HEC-RAS model computes flood depths by subtracting the WSE, interpolated between cell faces, from the high-resolution terrain. However, we have not subtracted the low-resolution WSE, calculated from the HydroPol2D outputs, from high-resolution terrain. When applying this approach to raster-based models, which generate low-resolution depths derived from resampled terrain, the resulting flood maps are often unrealistic. During the bilinear operation, a group of elevation pixels is represented by a single weighted distance average. When the low-resolution WSE is subtracted from this

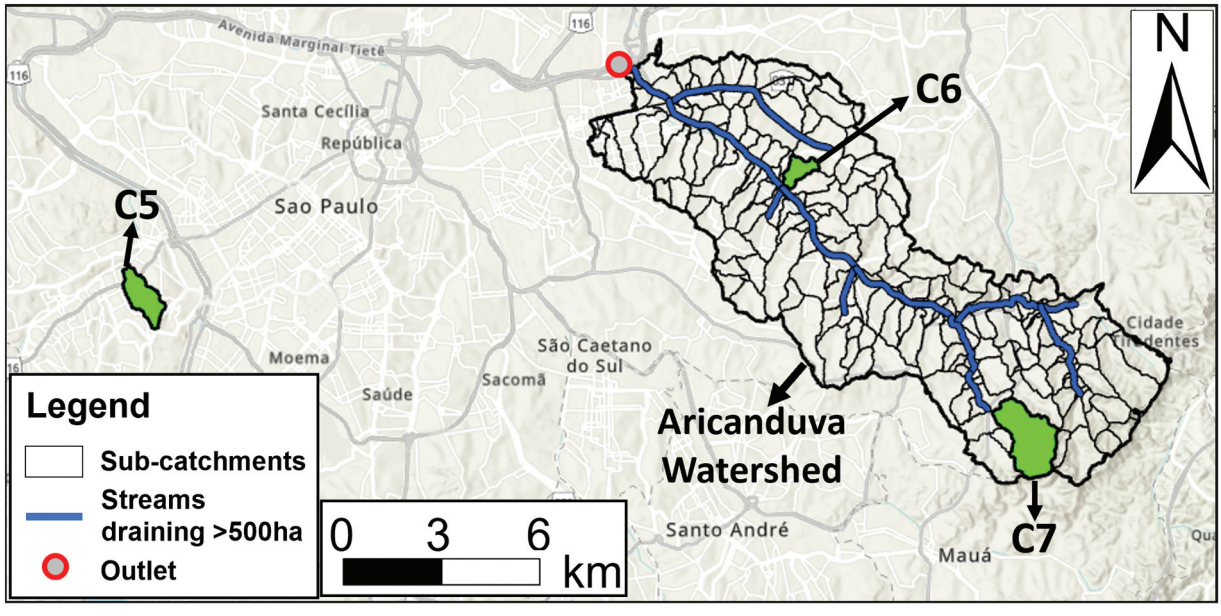

Figure 3. Aricanduva watershed and testing areas in Sao Paulo.

averaged value, only the lowest elevation cells within each of these coarse cells are depicted as flooded, while higher elevation cells incorrectly remain dry. Moreover, this averaging effect can sometimes produce flood depths that are unrealistically deep. This happens in areas where the original, finer-resolution terrain had significantly lower elevations than what is represented in the resampled coarser cell.

The flood volume v_t used for redistributing with cGAN-Flood was calculated directly from the maximum water depth maps. Unlike HEC-RAS, which interpolates WSE between cell faces, the water depths calculated with HydroPol2D result directly from the water balance between cells. The flood volume at each cell can be calculated by multiplying the cell's area by the water depth. Therefore, v_t is the sum of flood volume in each cell inside a given area. The method of calculating v_t for raster-based models makes it more accessible than mesh-based ones, which can be performed directly from low-resolution flood maps and does not require one of the model's source files, such as HEC-RAS hdf plan file.

2.4.1 Performance analysis in Sao Paulo catchments

The performance of cGAN-Flood coupled with HydroPol2D was also evaluated in smaller catchments instead of the whole Aricanduva watershed. Hyrodpol2D models with 15 m resolution were created for catchments C5, C6 and C7, located across Sao Paulo city (Fig. 3). The low-resolution HydroPol2D models were used to calculate v_t to be redistributed. These catchments were selected to represent different catchment sizes, imperviousness percentages, and average slopes, as presented in Table 1. HEC-RAS models with cell sizes of 3 m were created as ground truth for comparing modelling results.

Considering these catchments are situated outside San Antonio, the location of cGAN-Flood training catchments, we also assessed the transferability of cGAN-Flood to these different regions. Consequently, we compared the outputs from cGAN-Flood with the total flood volume (v_t) computed directly from the high-resolution HEC-RAS models. By doing this, we were able to eliminate the uncertainties associated with HydroPol2D in calculating v_t from this analysis. As a result, we can gain a more precise understanding of the errors that are exclusively associated with the cGAN-Flood model.

2.5 Performance metrics

We used a combination of the mean absolute error (MAE), root mean square error (RMSE), and the Nash-Sutcliffe efficiency (NSE) to assess the spatial accuracy of low-resolution flood maps with and without applying cGAN-Flood, for all cells with depths equal to or greater than 0.01 m. We also utilized the hit rate (HR), false alarm rate (FAR), and critical success index (CSI) to evaluate the accuracy of the predicted flooded areas. The formulas for these metrics are as follows:

$$\mathrm{HR} = \frac{\mathrm{Hits}}{\mathrm{Hits} + \mathrm{False\ Alarms}} \tag{1}$$

$$\mathrm{FAR} = \frac{\mathrm{False\ Alarms}}{\mathrm{Hits} + \mathrm{False\ Alarms}} \tag{2}$$

$$\mathrm{CSI} = \frac{\mathrm{Hits}}{\mathrm{Hits} + \mathrm{False\ Alarms} + \mathrm{Misses}} \tag{3}$$

In this context, 'hits' represent cells identified as flooded by both models, 'false alarms' denote cells flagged as flooded solely by cGAN-Flood, and 'misses' are cells recognized as flooded exclusively by the high-resolution HEC-RAS. We adopted thresholds of 0.01, 0.05, and 0.3 m for distinguishing between dry and wet cells, in line with previous flood studies (Brown *et al.* 2007, Guidolin *et al.* 2016, Jamali *et al.* 2018, Löwe *et al.* 2021, Shi *et al.* 2021), to better evaluate the performances under different depth magnitudes. HR and FAR were calculated only for a threshold of 0.05 m, which is the middle magnitude of the selected ones. The CSI metric was calculated with depth thresholds (CSI_{1cm}, CSI_{5cm}, and CSI_{30cm}), as this measurement accounts for both false alarms and misses.

3 Results and discussion

3.1 Model performance for the Upper San Antonio watershed

First, we evaluated the capability of the low-resolution HEC-RAS model to predict maximum flood volumes. Table 2 shows that the volume calculated with the low-resolution HEC-RAS

Table 1. Characteristics of test catchments in Sao Paulo.

Location	Area (ha)	Number of cells (× 10^3)	Average cell slope (°)	Impervious area (%)
C5	128	142	33	76.3
C6	63	70.4	28	91.5
C7	303	336.8	50	31

Table 2. Comparison of total flood volume calculated from low- and high-resolution HEC-RAS models.

Storm	Catchment	Volume high-resolution HEC-RAS (1000 m^3)	Volume low-resolution HEC-RAS (1000 m^3)	Error (%)
25-year	C1	116.5	104.3	−10.4
	C2	289.8	273.5	−5.6
	C3	118.9	113.7	−4.4
	C4	223.9	211.9	−5.3
100-year	C1	139.4	125.6	−9.9
	C2	348.8	330.3	−5.3
	C3	142.7	132.8	−6.9
	C4	270.6	255.3	−5.6

Table 3. Performance metrics of low-resolution HEC-RAS and cGAN-Flood compared to high-resolution HEC-RAS.

Model	Storm	Catchment	FAR	HR (%)	CSI_{5cm} (%)	CSI_{1cm} (%)	CSI_{30cm} (%)	RMSE (m)	MAE (m)	NSE
Low-resolution HEC-RAS and cGAN-Flood	25-year	C1	23	90	71	83	74	0.07	0.013	0.75
		C2	23	91	72	80	61	0.07	0.019	0.70
		C3	19	90	74	84	66	0.06	0.014	0.76
		C4	19	87	72	80	63	0.09	0.013	0.73
	100-year	C1	20	90	73	84	76	0.07	0.014	0.78
		C2	22	92	73	81	62	0.08	0.022	0.72
		C3	17	91	76	86	65	0.07	0.016	0.77
		C4	17	88	75	82	66	0.08	0.014	0.75
Low-resolution HEC-RAS	25-year	C1	27	40	35	30	67	0.05	0.018	0.67
		C2	17	47	43	35	62	0.07	0.023	0.64
		C3	15	46	42	36	57	0.06	0.022	0.63
		C4	23	49	42	35	51	0.07	0.019	0.59
	100-year	C1	14	37	35	28	78	0.05	0.016	0.74
		C2	15	48	44	36	62	0.07	0.026	0.66
		C3	13	50	46	41	60	0.06	0.023	0.67
		C4	19	49	44	36	55	0.08	0.021	0.63

model, which was used as input to cGAN-Flood, matches the volume predicted with high-resolution HEC-RAS relatively well. The largest error was an underestimation by approximately 10% for catchment C1 (25-year storm). The average error of all simulations is −6.7%. This table also demonstrates that low-resolution HEC-RAS tends to underestimate flood volume, meaning that the stormwater flows out of the catchment faster than simulated with a high-resolution model. One possible explanation is leakages from the coarse cells, which cause water to skip high-ground terrains and reach the outlet faster.

Flood maps were created for the four sub-catchments in the UPSA watershed with low- and high-resolution HEC-RAS models and with cGAN-Flood. Table 3 shows the metrics for the low-resolution and cGAN-Flood outputs for the 25 and 100-year storms. When comparing the two models, based on the FAR, HR, and CSI, we observe that cGAN-Flood generally outperforms

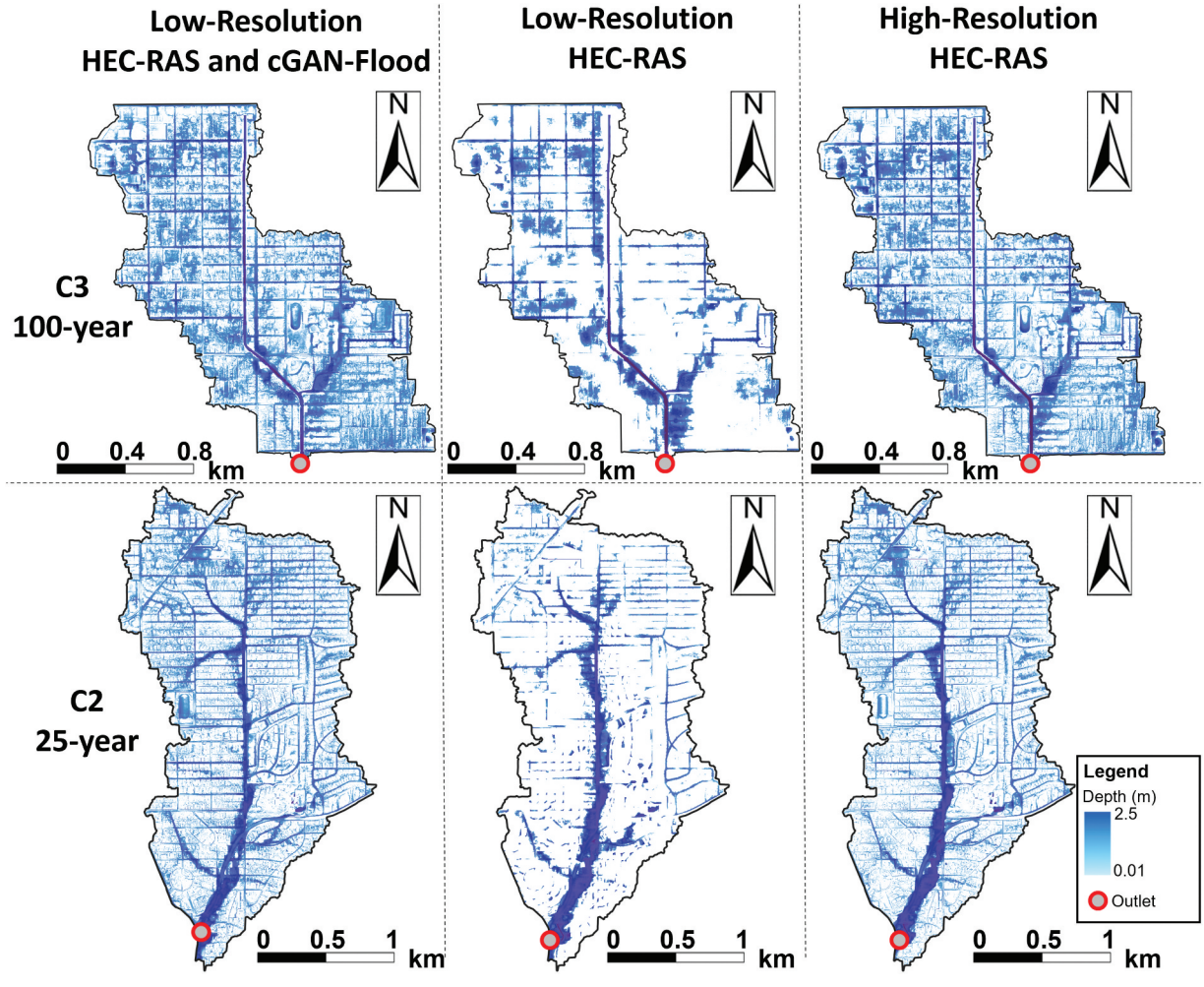

Figure 4. Low-resolution HEC-RAS and cGAN-Flood flood maps compared to high-resolution HEC-RAS.

low-resolution HEC-RAS, except for FAR. Figure 4 illustrates flood mapping outputs from the low-resolution HEC-RAS and cGAN-Flood, which indicates that the DL model significantly improved flood mapping.

The cGAN-Flood could improve the HR, CSI_{5cm}, and CSI_{1cm} by 44%, 31%, and 48%, respectively, in comparison to the low-resolution HEC-RAS model. The improvement in CSI_{30cm} (deeper depths) was less significant, about 5%. The reason is that deeper water is more frequently present along the channel, which was better captured in the low-resolution HEC-RAS model, demonstrated by better CSI_{30cm} metrics compared to CSI_{5cm} and CSI_{1cm}. Furthermore, cGAN-Flood tends to show lower performance when analysing CSI_{30cm} (Do Lago *et al.* 2023). For FAR, which measures the proportion of false positives among the total predicted positives, low-resolution HEC-RAS consistently has a lower average FAR (with an average of 18%) across all locations compared to cGAN-Flood (an average of 20%). The reason is that HEC-RAS consistently underestimated shallower depths across these sub-catchments, reducing false negatives.

In addition to improving the flooded areas, cGAN-Flood also improved the flood depths across the domains, as demonstrated by the MAE and NSE. The DL model decreased the MAE from an average of 0.15 to 0.13 m and improved the NSE from 0.66 to 0.75. Figure 5 illustrates the difference between the cGAN-Flood and low-resolution HEC-RAS, and the high-resolution HEC-RAS. It can be observed that, in general, the errors are closer to zero with cGAN-Flood when compared to low-resolution HEC-RAS. However, Fig. 5 also shows that cGAN-Flood presented some localized areas with more expressive errors (e.g. near the outlet of area C4). When comparing low- and high-resolution HEC-RAS outputs, the flood depths are expected not to deviate significantly, as we are comparing outputs generated with the same set of hydrodynamic equations and solver algorithm. Consequently, the RMSE increased by an average of 0.008 m after applying

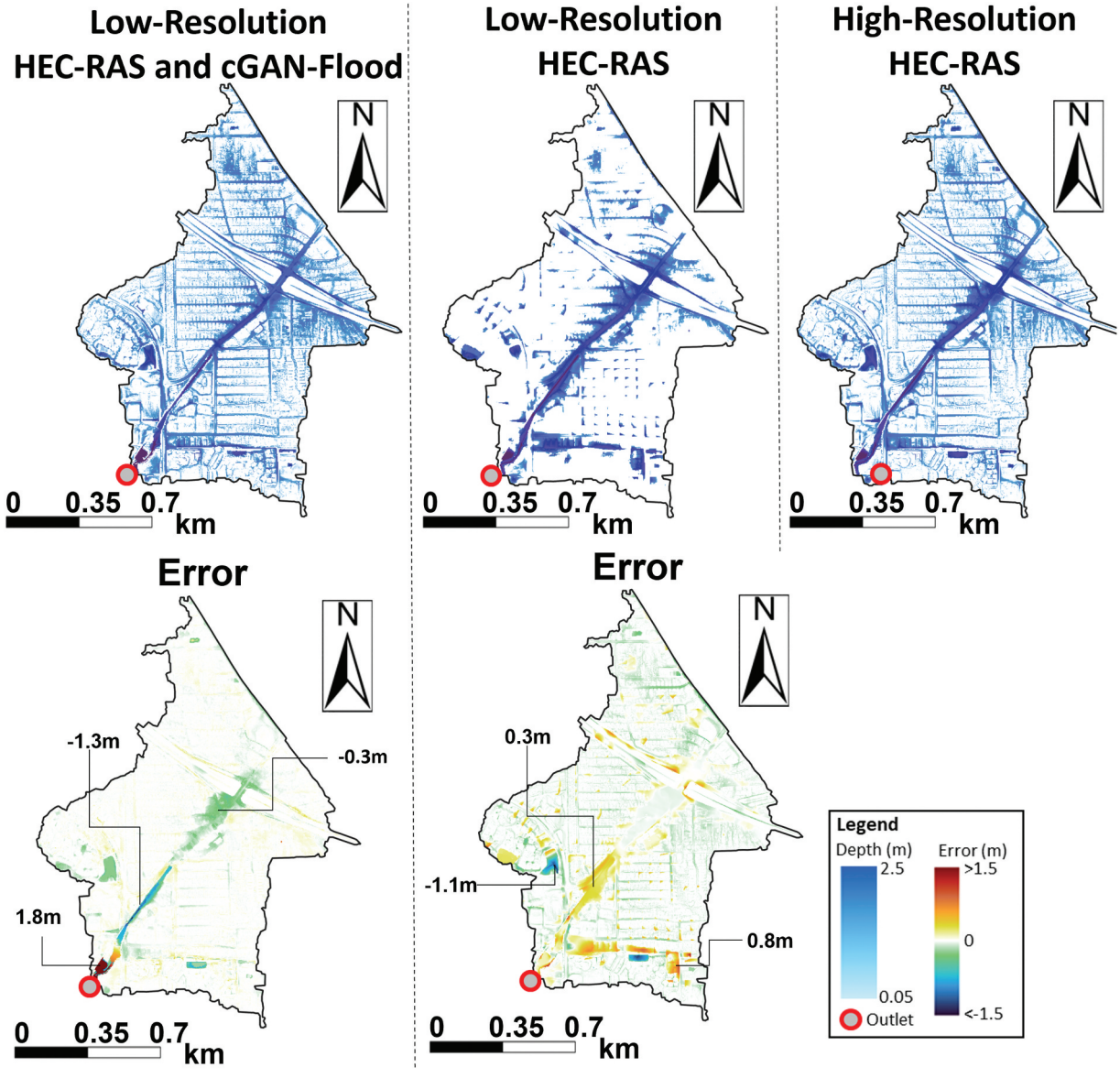

Figure 5. Depth errors of low-resolution HEC-RAS and cGAN-Flood compared to high-resolution HEC-RAS.

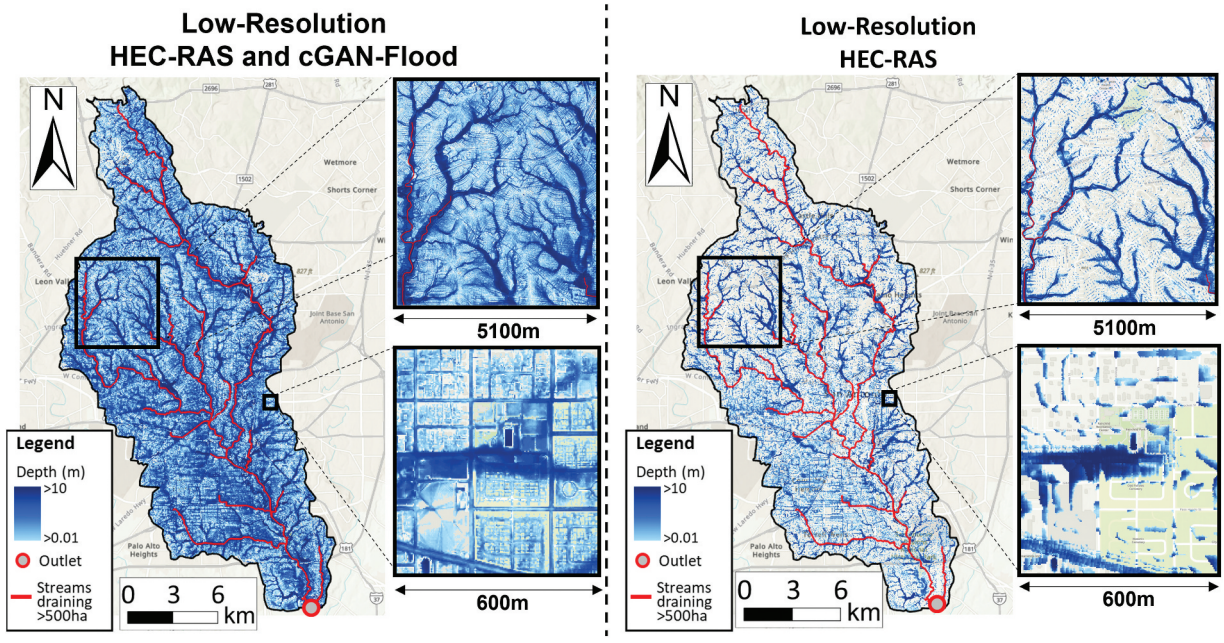

Figure 6. Flood maps of the entire UPSA watershed with a low-resolution HEC-RAS model and after coupling it with cGAN-Flood. Depths are visualized with an equalized histogram for better illustration.

cGAN-Flood, as the more significant errors are magnified with the root operation of this metric.

3.1.1 High-resolution prediction for the UPSA watershed

The comprehensive flood maps produced by the low-resolution HEC-RAS model, enhanced by the cGAN-Flood volume redistribution, are displayed in Fig. 6. Integrating a low-resolution hydrodynamic model and cGAN-Flood led to significant enhancements in flood map predictions throughout the UPSA watershed, particularly in depicting shallower depths. Such details regarding shallow cells can provide valuable insights to local authorities during emergencies. For instance, vehicular aquaplaning can occur at speeds of 70 or 62 km/h when water depths reach 0.01 and 0.02 m, respectively (Oh *et al.* 2008). More precise flood maps can enhance the effectiveness of responses, such as evacuation strategies, and contribute to safeguarding local residents.

From a time efficiency perspective, the low-resolution HEC-RAS model (570 000 cells) required 31 min, while the cGAN-Flood volume redistribution across the entire UPSA took an additional 37 min. Therefore, the total computation time to generate high-resolution flood maps for about 38 million cells was 68 min, or 0.1 ms/cell. In comparison, the prediction of a 25-year flood map in area C1, with approximately 150 000 cells, took 37 min (14.8 ms/cell). Notably, the simulation time per cell decreases with a low-resolution model, as the coarser model decreases the Courant number and allows for larger time steps. If we presume that the computation time scales with the number of cells, a rough estimate suggests that a full HEC-RAS simulation with a 3 m resolution for the UPSA would take approximately 160 h (or nearly one week), assuming the simulation time per cell is equivalent to that of area C1. These results underscore the potential of DL models for enhancing efficiency in large-domain predictions. However, it is worth noting that the fluvial flooding in segments draining over 500 ha was calculated with 15 m cells in the low-resolution model HEC-RAS model. Applying finer cell sizes or a combination with a 1D HEC-RAS can improve the flood predictions at these locations, which can affect the total simulation time. HEC-RAS 1D models have been traditionally used for fluvial flood predictions and may be a preferred option for rapid flood modelling as they are less computationally demanding.

3.2 Model performance in Sao Paulo

The effectiveness of cGAN-Flood in Sao Paulo catchments was evaluated by comparing its outputs with the HEC-RAS map. To exclude uncertainties related to predicting the flood volume, the flood volume distributed with cGAN-Flood exactly matches the volume in HEC-RAS maps for this first analysis. As the

Table 4. Performance metrics for catchments in Sao Paulo.

Storm	Catchment	HR (%)	FAR (%)	CSI_{5cm} (%)	CSI_{1cm} (%)	CSI_{30cm} (%)	RMSE (m)	MAE (m)	NSE
10-year	C5	76	21	63	69	50	0.17	0.09	0.65
	C6	83	23	67	73	49	0.09	0.05	0.70
	C7	78	28	60	61	53	0.19	0.11	0.70
100-year	C5	77	19	66	72	54	0.17	0.10	0.68
	C6	84	21	69	75	54	0.09	0.06	0.72
	C7	77	25	61	62	58	0.21	0.12	0.71

characteristics of catchments C5, C6, and C7 are significantly different from those of the training catchments, cGAN-Flood showed worse performance here than with testing catchments in San Antonio. For instance, the average RMSE and MAE were 0.15 and 0.09 m for C5, C6, and C7, while the maximum values for the catchments at UPSA were 0.09 and 0.019 m. The maximum NSE in Sao Paulo was 0.72, below the average of 0.75 for UPSA catchments.

CSI also shows larger errors regarding flooded cell locations in Sao Paulo than in San Antonio, as Table 4 shows. cGAN-Flood showed better accuracy when considering shallow depths, similar to UPSA catchments, with higher CSI_{1cm} values than CSI_{5cm} and CSI_{30cm}. CSI_{30cm} presented the lowest values, with an average of 53%. Higher CSI values considering shallower depths were also observed in (Löwe *et al.* 2021). For instance, their CSI_{5cm} ranged from 44.7 to 58.3% (average of 48.7%), and their CSI_{30cm} ranged from 23.5 to 59.2% (average of 37.4%).

A comparison between Tables 4 and 6 shows noteworthy dynamics in catchments C5, C6, and C7 concerning flood volume and the impacts of errors in calculating v_t on the performance metrics. In catchments C5 and C6, we observed a decrease in flood volume, which led to a decrease in both HR and FAR. In contrast, catchment C7 exhibited the opposite trend, where an increase in flood volume was observed. This relationship between flood volume and the model's performance reflects how flood volume distribution affects the predicted flooded area. Generally, a lower volume of floods to distribute tends to decrease the overall flooded area. This reduction in flooded area decreases the likelihood of the model incorrectly predicting a flooded cell, thereby reducing the FAR. This is evident in catchments C5 and C6, where the decreased flood volume led to a reduced FAR, indicating fewer false positives in flood prediction. However, this decrease in flood volume also has also an impact on the HR metric. With less flood volume being distributed, the model tends to underestimate the actual flooded area. This underestimation results in fewer cells being correctly modelled as flooded, adversely affecting the HR metric. It indicates that while the model becomes more conservative in predicting flood occurrence (hence lower FAR), it also becomes less effective in identifying all the areas that should be flooded (lower HR).

The different spatial inputs between San Antonio and Sao Paulo catchments explain the drop in performance. First, Sao Paulo city is more hilly, with the average cell slope of the terrain in the selected areas varying from 28 to 50°. As a comparison, the catchments with the highest average cell

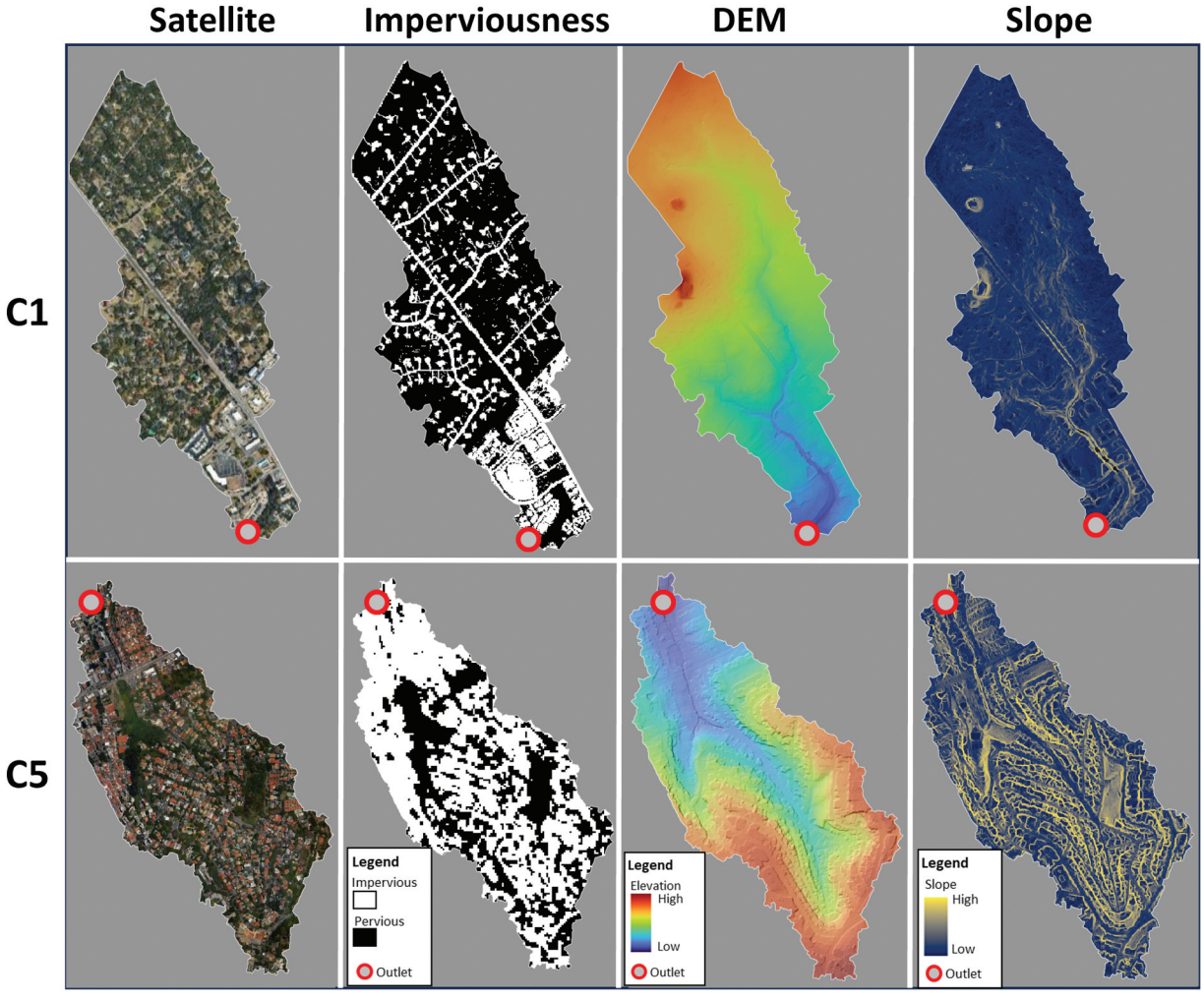

Figure 7. Illustration of the difference in spatial characteristics between San Antonio and Sao Paulo.

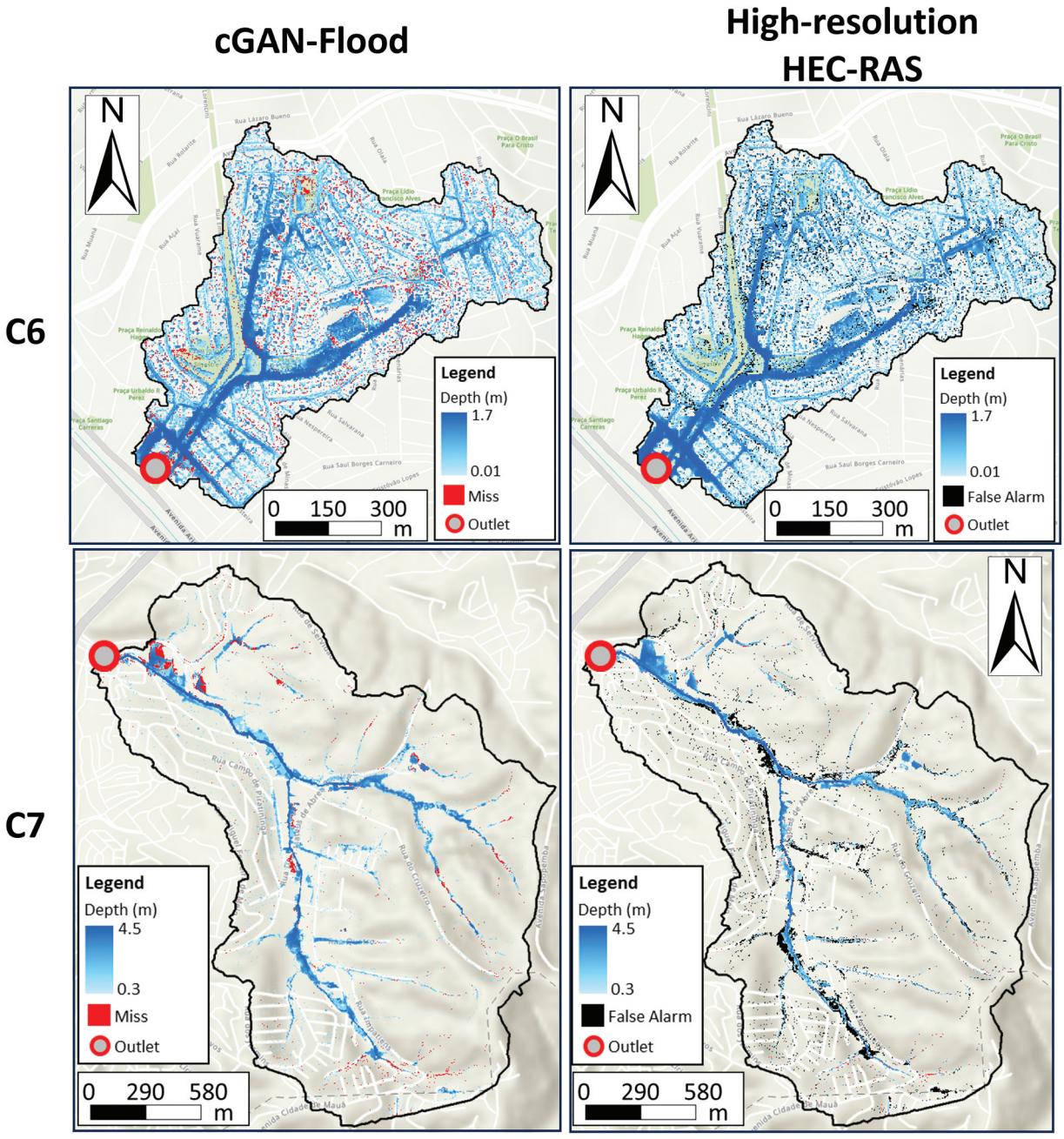

Figure 8. Examples of cGAN-Flood performance on Sao Paulo catchments with depth thresholds of 0.05 and 0.3 m.

slope used during the training phase was 21°, which includes the terrain modification used for data augmentation (Do Lago *et al.* 2023). Furthermore, Sao Paulo tends to have fewer green spaces compared to San Antonio. For instance, C5 and C6 present an imperviousness percentage higher than all testing, validating, and training catchments in San Antonio, which ranged from 29.9 to 63.8% Do Lago *et al.* (2023). C7 is located in a suburban area with only 31% impervious area. In addition, the spatial patterns of the input data in Sao Paulo differ from what cGAN-Flood saw during training. Figure 7 illustrates the spatial inputs in San Antonio and Sao Paulo catchments, represented by C1 and C5, respectively. The first major difference is the imperviousness data. In San Antonio, the high resolution allows for delineating roads and buildings. In Sao Paulo, however, an imperviousness map with only a 10 m resolution is available, with the impervious areas represented as continuous blocks. It can also be seen that the terrain model in San Antonio is smoother than the one in Sao Paulo, which presents more abrupt changes in elevation due to terrain excavations to accommodate housing. These differences in terrain also affect the slope matrixes with patterns that were unseen during training.

Despite the drop in performance, cGAN-Flood could still generate reasonable flood maps for Sao Paulo catchments. Figure 8 exemplifies flood predictions for catchments C6 and C7 for depths greater than 0.01 and 0.3 m. In catchment C6, the cGAN-Flood map was similar to the HEC-RAS output, with sparse miss and false alarm cells across the catchments. cGAN-Flood tends to overestimate the number of cells equal to or larger than 0.3 m, especially along the main channel. The reason

Table 5. Comparison of total flood volume calculated from high-resolution HEC-RAS and low-resolution Hydropol2D models.

Storm	Catchment	Volume high-resolution HEC-RAS (1000 m^3)	Volume low-resolution Hydropol2D (1000 m^3)	Error (%)
10-year	C5	102.1	94.6	−7.3
	C6	33	29.9	−9.3
	C7	196.4	224	14.1
100-year	C5	124.6	116.9	−6.2
	C6	40.4	36.4	−9.8
	C7	246.2	299.4	21.6

Table 6. Performance metrics of low-resolution Hydropol2D and cGAN-Flood.

Model	Storm	Catchment	FAR (%)	HR (%)	CSI_{5cm} (%)	CSI_{1cm} (%)	CSI_{30cm} (%)	RMSE (m)	MAE (m)	NSE
Low-resolution Hydropol2D and cGAN-Flood	10-year	C5	19	73	63	69	52	0.09	0.17	0.66
		C6	20	80	67	73	48	0.05	0.09	0.70
		C7	31	80	59	61	50	0.12	0.19	0.67
	100-year	C5	17	76	65	71	55	0.10	0.18	0.68
		C6	18	82	69	75	54	0.06	0.10	0.72
		C7	30	80	60	61	52	0.14	0.23	0.66
Low-resolution Hydropol2D	10-year	C5	36	28	24	41	32	0.13	0.16	0.36
		C6	30	39	33	43	41	0.07	0.06	0.51
		C7	36	44	35	35	38	0.13	0.17	0.40
	100-year	C5	34	33	28	45	36	0.13	0.17	0.40
		C6	29	42	36	47	46	0.07	0.07	0.54
		C7	33	49	40	35	47	0.12	0.19	0.45

might be the higher slope of the catchment when compared to the training ones, and cGAN-Flood underestimated the channel's flow capacity. Nonetheless, cGAN-Flood could still identify the main flood locations in C7.

The errors in flood volume prediction when coupling HydroPol2D with cGAN-Flood are presented in Table 5. The error in v_t calculated with the low-resolution HydroPol2D varied from −9.8% to 21.6%. Catchments C5 and C6 presented errors comparable to those related to the ones calculated with low-resolution HEC-RAS, ranging from −6.2 to −9.8%. Volumes calculated for C7 were significantly higher, possibly due to high catchment slopes. As a rapid flood model, HydroPol2D does not consider inertia, which is relevant for accurate predictions in areas with high velocities (Jamali *et al.* 2018).

The performance of cGAN-Flood when integrated with HydroPol2D is detailed in Table 6. Generally, a decrease in the performance of cGAN-Flood is observed when it is coupled with HydroPol2D, primarily due to errors in the calculation of v_t. For example, the FAR in Catchment C7 was observed to be 31 and 30%, attributed to an overestimation in flood volume, as opposed to 28 and 25% when the volumes are well matched (refer to Table 4). However, when we average the metrics for the three catchments across both the 10- and 100-year storm events, the degradation in performance is not substantial. Specifically, the averages for CSI_{5cm} and NSE declined slightly, from 64 to 63% and from 0.69 to 0.68, respectively, while the average RMSE increased marginally, from 0.15 to 0.16. This analysis indicates that errors tied to the performance of the DL model in redistributing the flood volume are more significant than errors in the calculation of flood volume. This underscores the necessity to expand the training of the cGAN-Flood model to enable it to recognize a wider array of spatial patterns, thereby enhancing its generalization capabilities.

In spite of the errors linked to cGAN-Flood and flood volume prediction, the integration of the DL model with the low-resolution HydroPol2D model substantially enhanced the precision of flood predictions compared to HydroPol2D alone. For example, HydroPol2D significantly underestimates flooded cells with a depth greater than 0.05 m, with HR values ranging between 28 and 49%. However, upon coupling with cGAN-Flood, HR values increased to fall within the range of 73 to 82%. The incorporation of cGAN-Flood resulted in an average decrease in FAR and RMSE by 10.5% and 0.015 m, respectively, and an average increase in CSI_{1cm} and NSE by 27% and 0.25, respectively. The MAE presented an average increase of 0.02 m. The advancement in flood mapping resolution is depicted in Fig. 9. Despite a significant error of 21% in volume prediction for catchment C7, the flood maps generated with the use of cGAN-Flood are noticeably more accurate compared to those produced by the low-resolution HydroPol2D. Notably, the low-resolution simulation from HydroPol2D failed to capture essential flood features such as roads, a shortcoming attributable to the resampling of the terrain. These findings also suggest that the flooded area (with depths greater than 0.01 m) is generally greatly overestimated. This pattern may explain why MAE is lower with the low-resolution HydroPol2D. Shallow depths overestimated by HydroPol2D are registered as zero with HEC-RAS outputs. At these locations, the discrepancy between cell depths is relatively minimal, resulting in a reduction of the MAE.

In addition to the cGAN-Flood errors analysed in this paper, there is also the uncertainty related to the inputs to the hydrodynamic models, particularly regarding the values for infiltration and surface roughness used in HEC-RAS and HydroPol2D. These parameters are significant in determining the flood volume to be redistributed, which in turn influences the outputs of cGAN-Flood, as previously discussed. To gain a deeper understanding of how the infiltration and roughness factors affect the model's outputs, a sensitivity analysis can be performed to analyse how the variations in these parameters alter the flood predictions. Additionally, it is important to assess the accuracy and uncertainties of our methods with

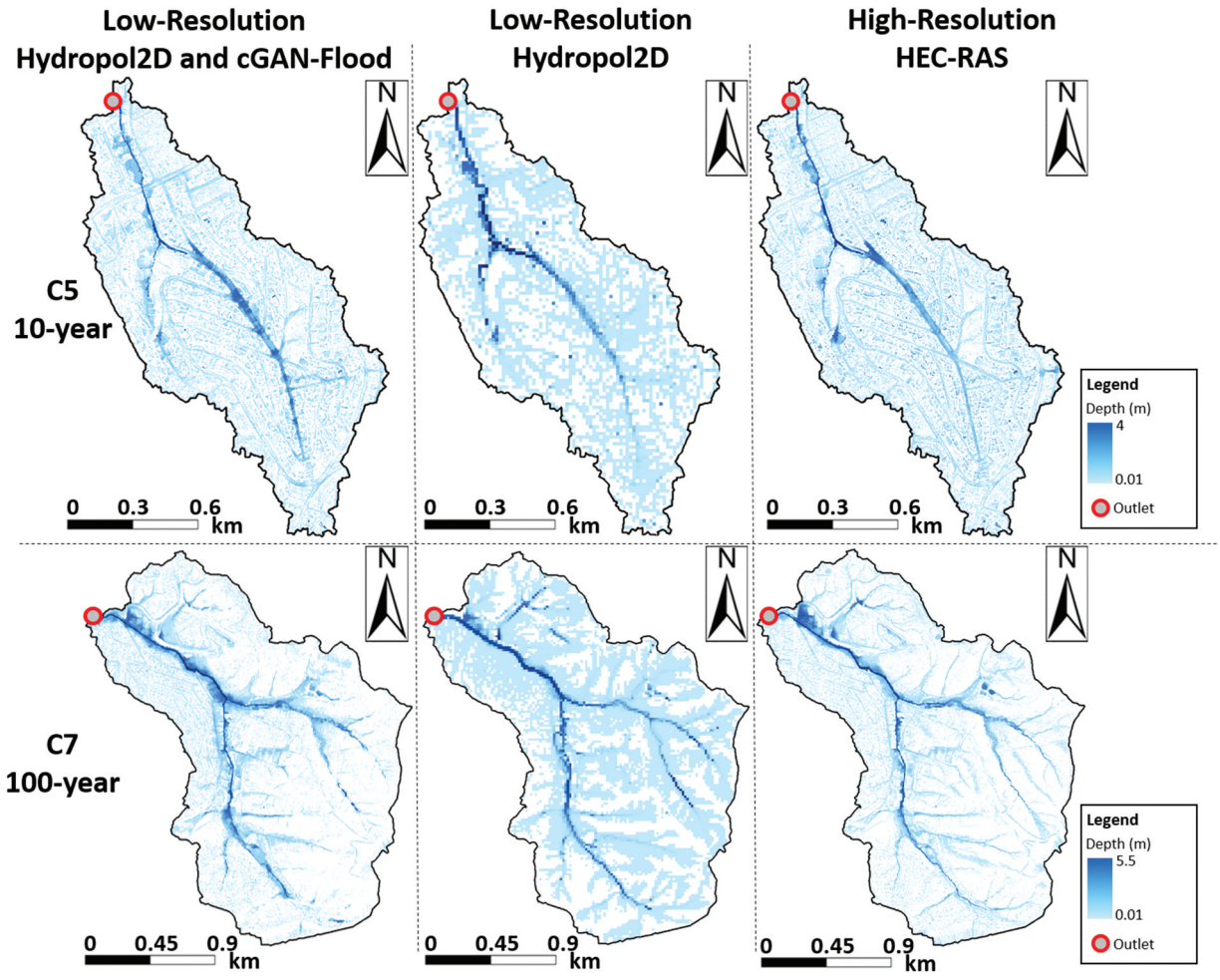

Figure 9. Flood maps generated with cGAN-FLood and low-resolution Hydropol2D compared with high-resolution HEC-RAS.

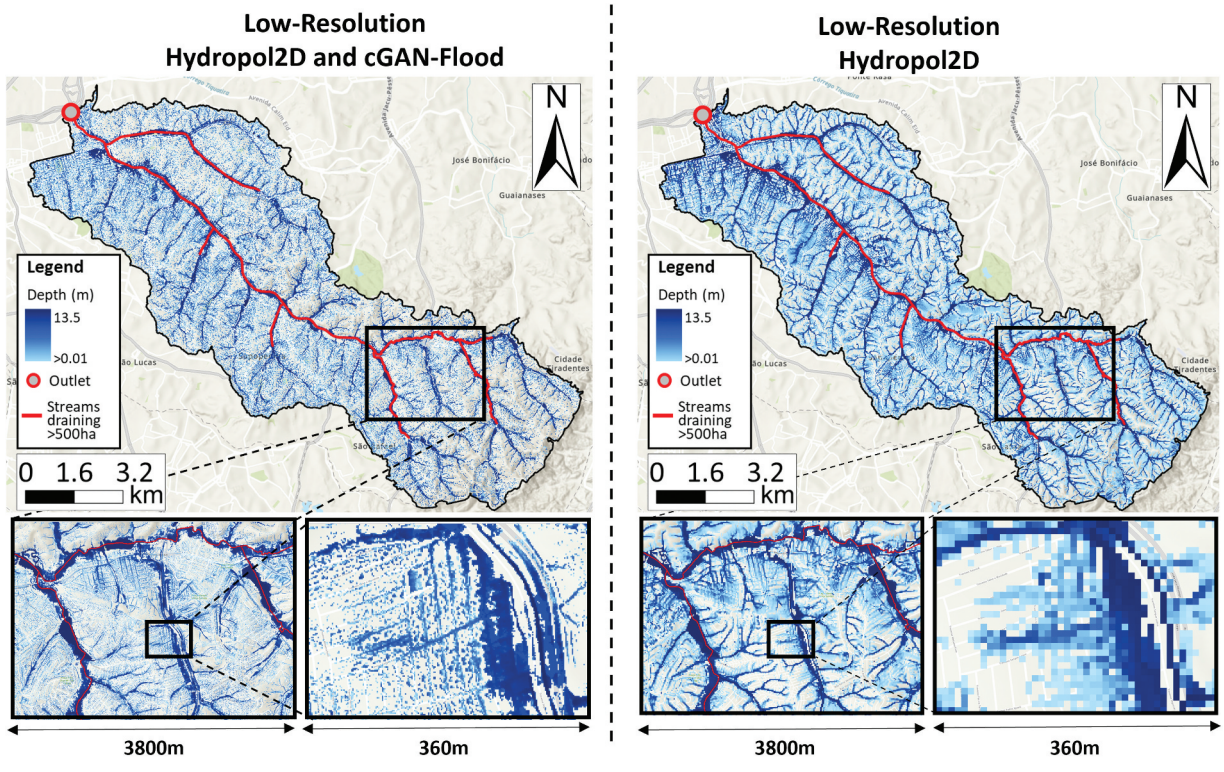

Figure 10. Flood maps of the entire Aricanduva watershed with a low-resolution Hydropol2D model and after coupling it with cGAN-Flood.

observational data from historical flood events. By analysing the differences between the model's predicted flood extents and depths and actual observed data, we can identify the areas where the model may exhibit uncertainty.

3.2.1 High-resolution prediction for the Aricanduva watershed

The improvements in flood mapping resolution of HydroPol2D maps with cGAN-Flood for Aricanduva watershed are exemplified in Fig. 10. Unlike the flood maps generated with the low-resolution mesh-based model, which failed to generate pluvial flooding (Fig. 10), the low-resolution HydroPol2D could somewhat represent flood patterns with the coarse pixel size. However, as discussed in the previous section, resampling the terrain may misrepresent important urban features, such as roads, leading to overestimating shallow depths. Redistributing the flooded volume with cGAN-Flood to a higher resolution results in a more realistic prediction of flooded depth and area.

Regarding time efficiency, the low-resolution HydroPol2D model, comprising 460 000 pixels with 15 m resolution, demanded 75 min, while the cGAN-Flood volume redistribution across the entire Aricandura watershed took an additional 18 min. Consequently, the total computation time to create high-resolution flood maps encompassing roughly 11.5 million cells was 83 min (0.4 ms/cell). Considering the same assumption of computational efficiency discussed in 3.1.1, a high-resolution HEC-RAS model with a 3 m cell size would take approximately 2 days of simulation for the Aricanduva watershed. This analysis highlights the potential of increasing the resolution of coarse flood maps derived from a raster-based model.

In rapid flood modelling, predicting solely the maximum flood depths is an approach used for time efficiency, bypassing intermediate steps to achieve faster results (Jamali *et al.* 2018, 2019). However, the lack of temporal evolution is a disadvantage when compared to hydrodynamic models, which can be significant for real-time predictions. While cGAN-Flood theoretically has the capability to generate flood maps at specific times, this diminishes its computational time advantage, as separate simulations are needed for each required map. However, each additional map created with cGAN-Flood accumulates extra simulation time, equivalent to the DL processing duration. For example, in the UPSA, generating each additional flood map would require an extra 37 min, while in the Aricanduva area, this would add about 18 min per map.

4 Conclusions and future model improvements

This study addressed an important gap regarding flood predictions for large domains, demonstrating a pioneering application of deep learning (DL) models to enhance flood mapping resolution originating from coarse hydrodynamic models. This presents a significant leap towards refining flood modelling while maintaining computational feasibility. Our work showcased the use of cGAN-Flood with two types of coarse flood models, mesh- and raster-based, feeding the total volume to be distributed. Our approach has underscored the potential to ameliorate the resolution of flood mapping in pre-existing 2D hydrodynamic models.

The generalization capacity of cGAN-Flood allowed its application for large-scale prediction without the need to train the DL model for the entire area. Training the DL model for the entire area would be challenging, as it would require building several hydrodynamic models to cover the whole watershed. Furthermore, the training process can often be complex and time-demanding. Despite the significant changes from the training areas, cGAN-Flood could predict flood maps in Sao Paulo catchments. These results suggest that cGAN-Flood has a strong generalization capability. Training cGAN-Flood with a high variety of catchments can make its prediction performance consistently accurate across different regions and countries. This advantage enables the possibility to train a DL model in regions where substantial investments have been made in flood model development and subsequently apply the model in regions where such investments are deficient (e.g. areas with low population density or in developing countries).

cGAN-Flood has limitations, and future research is needed to improve its applicability. First, the model was not trained to account for underground drainage systems. Incorporating such systems in the model could improve its predictions, especially in urban settings where these systems are prominent and significantly influence flood dynamics. We also noted a relatively high FAR, particularly in the Sao Paulo catchments, despite underestimating the total volume to be distributed (v_t). This observation indicates a need to enhance the model's performance to reduce FAR and improve flood mapping.

Furthermore, cGAN-Flood is strictly confined to a 3 m raster resolution. The inability to adapt to finer or coarser cells restricts its application in situations where data resolution varies or in scenarios requiring more detailed flood predictions. Further adaptations should enable the model to work with different resolutions, broadening its application scope. Another disadvantage is that cGAN-Flood cannot predict velocities, a critical parameter for creating risk maps. Also, cGAN-Flood has only been trained under flood expansion. This gap presents an opportunity for further research and development, aiming to enhance the model's ability to simulate the full cycle of flood events, including both the rise and fall of water levels, to enable a better representation of the temporal evolution of flooding. Additionally, we suggest conducting a sensitivity analysis on infiltration and roughness parameters and comparing the model's predictions against observed data from past flood events to identify and better understand the uncertainties in our methods. Finally, this DL modelling approach can only be applied in drainage areas smaller than 500 ha, and fluvial flooding predictions in channels conveying stormwater from larger areas must be generated by an alternative method (e.g. 1D models). Although 1D modelling is accurate and computationally efficient in predicting fluvial flooding, building 1D hydrodynamic models requires significant investments and data. Coupling cGAN-Flood with a DL developed for fluvial predictions is recommended as a cheaper and faster alternative.

Acknowledgements

The authors thank Capes-Proex for funding this study.

Disclosure statement

No potential conflict of interest was reported by the author(s).

Funding

This work was supported by the Coordenação de Aperfeiçoamento de Pessoal de Nível Superior [Capes-Proex].

ORCID

Marcus Nóbrega Gomes Junior http://orcid.org/0000-0002-8250-8195
Eduardo Mario Mendiondo http://orcid.org/0000-0003-2319-2773

References

Bentivoglio, R., *et al.*, 2022. Deep learning methods for flood mapping: a review of existing applications and future research directions. *Hydrology and Earth System Sciences*, 26 (16), 4345–4378. doi:10.5194/hess-26-4345-2022

Bentivoglio, R., *et al.*, 2023. Rapid spatio- temporal flood modelling via hydraulics-based graph neural networks. *EGUsphere*, 2023, 1–24.

Berkhahn, S., Fuchs, L., and Neuweiler, I., 2019. An ensemble neural network model for real-time prediction of urban floods. *Journal of Hydrology*, 575, 743–754. doi:10.1016/j.jhydrol.2019.05.066

Brown, J.D., Spencer, T., and Moeller, I., 2007. Modeling storm surge flooding of an urban area with particular reference to modeling uncertainties: a case study of canvey island, United Kingdom. *Water Resources Research*, 43 (6). doi:10.1029/2005WR004597

Brunner, G., 2016. *Hec-ras river analysis system, 2d modeling user's manual, version 5.0*. Davis: US Army Corps of Engineers, hydrologic engineering center.

Bulti, D.T. and Abebe, B.G., 2020. A review of flood modeling methods for urban pluvial flood application. *Modeling Earth Systems and Environment*, 6 (3), 1293–1302. doi:10.1007/s40808-020-00803-z

Cea, L. and Costabile, P., 2022. Flood risk in urban areas: modelling, management and adaptation to climate change. a review. *Hydrology*, 9 (3), 50. doi:10.3390/hydrology9030050

Chen, A.S., *et al.*, 2012. Multi-layered coarse grid modelling in 2d urban flood simulations. *Journal of Hydrology*, 470, 1–11.

De Paiva, R.C.D., *et al.*, 2013. Large-scale hydrologic and hydrodynamic modeling of the Amazon River basin. *Water Resources Research*, 49 (3), 1226–1243. doi:10.1002/wrcr.20067

Do Lago, C.A., *et al.*, 2023. Generalizing rapid flood predictions to unseen urban catchments with conditional generative adversarial networks. *Journal of Hydrology*, 618, 129276. doi:10.1016/j.jhydrol.2023.129276

Do Lago, C.A.F., *et al.*, 2021. Assessing the impact of climate change on transportation infrastructure using the hydrologic-footprint-residence metric. *Journal of Hydrologic Engineering*, 26 (5), 04021014. doi:10.1061/(ASCE)HE.1943-5584.0002076

Downer, C.W. and Ogden, F.L., 2004. Gssha: model to simulate diverse stream flow producing processes. *Journal of Hydrologic Engineering*, 9 (3), 161–174. doi:10.1061/(ASCE)1084-0699(2004)9:3(161)

Dtissibe, F.Y., *et al.*, 2020. Flood forecasting based on an artificial neural network scheme. *Natural Hazards*, 104 (2), 1211–1237. doi:10.1007/s11069-020-04211-5

Fewtrell, T., *et al.*, 2008. Evaluating the effect of scale in flood inundation modelling in urban environments. *Hydrological Processes: An International Journal*, 22 (26), 5107–5118. doi:10.1002/hyp.7148

Gomes, M.N., Jr, *et al.*, 2023. Hydropol2d–distributed hydrodynamic and water quality model: challenges and opportunities in poorly- gauged catchments. *Journal of Hydrology*, 625, 129982. doi:10.1016/j.jhydrol.2023.129982

Gonog, L. and Zhou, Y., 2019. A review: generative adversarial networks. *In: 2019 14th IEEE conference on industrial electronics and applications (ICIEA)*, Xi'an, China. IEEE. 505–510.

Guidolin, M., *et al.*, 2016. A weighted cellular automata 2d inundation model for rapid flood analysis. *Environmental Modelling Software*, 84, 378–394. doi:10.1016/j.envsoft.2016.07.008

Guo, Z., Moosavi, V., and Leitão, J.P., 2022. Data-driven rapid flood prediction mapping with catchment generalizability. *Journal of Hydrology*, 609, 127726. doi:10.1016/j.jhydrol.2022.127726

Hofmann, J. and Schüttrumpf, H., 2021. floodgan: using deep adversarial learning to predict pluvial flooding in real time. *Water*, 13 (16), 2255. doi:10.3390/w13162255

Jamali, B., *et al.*, 2018. A rapid urban flood inundation and damage assessment model. *Journal of Hydrology*, 564, 1085–1098. doi:10.1016/j.jhydrol.2018.07.064

Jamali, B., *et al.*, 2019. A cellular automata fast flood evaluation (ca-ff´e) model. *Water Resources Research*, 55 (6), 4936–4953. doi:10.1029/2018WR023679

Kabir, S., *et al.*, 2020. A deep convolutional neural network model for rapid prediction of fluvial flood inundation. *Journal of Hydrology*, 590, 125481. doi:10.1016/j.jhydrol.2020.125481

Karim, F., *et al.*, 2023. A review of hydrodynamic and machine learning approaches for flood inundation modeling. *Water*, 15 (3), 566. doi:10.3390/w15030566

Löwe, R., *et al.*, 2021. U- flood–topographic deep learning for predicting urban pluvial flood water depth. *Journal of Hydrology*, 603, 126898. doi:10.1016/j.jhydrol.2021.126898

Natarajan, S. and Radhakrishnan, N., 2019. Simulation of extreme event-based rainfall–runoff process of an urban catchment area using hec-hms. *Modeling Earth Systems and Environment*, 5 (4), 1867–1881. doi:10.1007/s40808-019-00644-5

Oh, C.W., *et al.*, 2008. Hydroplaning simulation for a straight-grooved tire by using fdm, fem and an asymptotic method. *Journal of Mechanical Science and Technology*, 22 (1), 34–40. doi:10.1007/s12206-007-1004-y

PMSP, S.P.P.M.D.S.P., 2017. *Portal geosampa*. Available from: http://geosampa.prefeitura.sp.gov.br/PaginasPublicas/SBC.aspx [Accessed 12 April 2022].

Rangari, V., Gonugunta, R., Umamahesh, N., Patel, A., Bhatt, C., 2018. 1d–2dmodelingofurbanfloodsandriskmapgenerationforthepartofhyderabadcity. TheInternationa–450. [Accessed 12 Apr 2022].

Rossman, L.A., 2010. Storm water management model user's manual.

Schwanghart, W. and Scherler, D., 2017. Bumps in river profiles: uncertainty assessment and smoothing using quantile regression techniques. *Earth Surface Dynamics*, 5 (4), 821–839. doi:10.5194/esurf-5-821-2017

Shi, Z., *et al.*, 2021. Development of integrated flooding early warning and rainfall runoff management platform for downtown area of shanghai. *Sustainability*, 13 (20), 11250. doi:10.3390/su132011250

Szewrański, S., *et al.*, 2018. Pluvial flood risk assessment tool (pfra) for rainwater management and adaptation to climate change in newly urbanised areas. *Water*, 10 (4), 386. doi:10.3390/w10040386

Teng, J., *et al.*, 2017. Flood inundation modelling: a review of methods, recent advances and uncertainty analysis. *Environmental Modelling Software*, 90, 201–216. doi:10.1016/j.envsoft.2017.01.006

Wang, K., *et al.*, 2017. Generative adversarial networks: introduction and outlook. *IEEE/CAA Journal of Automatica Sinica*, 4 (4), 588–598. doi:10.1109/JAS.2017.7510583

WBM, B., 2016. Tuflow user manual. *BMT WBM*.

Wolfram, S., 1984. Cellular automata as models of complexity. *Nature*, 311 (5985), 419–424. doi:10.1038/311419a0